# Multi-Channel Data Transmission with X Wave and Bessel Pulses



SUBMISSION DATE / POSTED DATE

13-02-2023 / 02-03-2023

CITATION

Lu, Jian-yu (2023): Multi-Channel Data Transmission with X Wave and Bessel Pulses. TechRxiv. Preprint. https://doi.org/10.36227/techrxiv.22083719.v2

DOI

10.36227/techrxiv.22083719.v2

# Multi-Channel Data Transmission with X Wave and Bessel Pulses

Jian-yu Lu, *Fellow*, *IEEE*

***Abstract*— X wave and Bessel pulses are waves that do not spread transversely as they propagate. When they are realized in practice with a wave radiator (such as transducer) of a finite aperture, they have a very large depth of field. Because of this property, they have various applications such as medical imaging.**

**In this paper, X wave and Bessel pulses were studied for ultrasound data transmission. Theory, computer simulation, and experiment were conducted. Both single-channel and multiple-channel data transmissions were investigated. Results show that it is feasible to use X wave and Bessel pulses to transmit information for data communication and the data transmission rate can be significantly increased over a large depth of field when multiple communication channels are used. This is important for applications such as video data transmission where a high data transmission rate is desirable.**

**In addition, applications of Bessel pulses as ultrasound or optical delay lines are discussed and the extension of applications of X wave to other waves such as optical, electromagnetic, and deBroglie waves are also discussed.**

***Index Terms*— X wave, Bessel pulses, ultrasound data communication, optical and electromagnetic communications, quantum mechanics, deBroglie waves, Klein-Gordon, Dirac, and Weyl equations**

[1]

## I. Introduction

Waves that do not spread transversely (in the direction that is perpendicular to the propagation direction) as they propagate have been studied by various researchers in different areas of science and engineering [1-17]. X wave (it is so called because its shape resembles the letter "X" along its axial cross section) [6-7] and Bessel pulses [14-16] are two examples of such waves that are highly localized as they propagate to infinite distance. In practice, when these waves are realized with a transmitter (such as an ultrasound transducer) of a finite aperture, they have a very large depth of field (DOF) (the distance at which the peak amplitude of the wave is reduced to one half of that at the surface of the wave source). Because of the nonspreading and localization property, both X wave and Bessel pulses have been used in various applications such as medical imaging [16, 18-19].

In this paper, X wave and Bessel pulses are studied for ultrasound data transmissions that have various applications. In underwater acoustics, ultrasound is used to communicate between submerged objects [20-21]. In industry, ultrasound is used to penetrate metal walls of containers for communications [22-23] where electromagnetic waves have difficulty to penetrate. In biomedical applications, ultrasound is used to communicate with implant or diagnostic devices [24-25]. In many of these applications, a high data transmission rate is desirable, especially, in applications where transmission of video signals is required.

In ultrasound communications, the data transmission rate is limited by many factors such as frequency, bandwidth, dispersion (wave speed changes with temporal frequency), diffraction, phase aberration, scattering, attenuation, multiple reflections, multiple paths, and noise, etc. Even under ideal conditions where the media is isotropic and homogeneous, the frequency, bandwidth, dispersion, and diffraction of ultrasound will ultimately limit the data transmission rate. Currently, conventional focused or unfocused ultrasound beams are used for data transmissions [20-25]. For unfocused beams such as spherical waves, ultrasound signal is spread in a wide space and thus its intensity drops quickly with distance due to diffraction. Also, the signals are easier to be intercepted and thus the communications are less secure. With focused beams, their DOF is short. I.e., the receiver needs to be placed near the focus of the beams to get the strongest signals. Away from the focus, the waves undergo diffraction spread and thus the wave intensity diminishes quickly.

Unlike focused beams, X wave and Bessel pulses have a very large DOF and are highly localized around the wave propagation axis. As the size of aperture of the transducer is increased, the DOF will increase proportionally. Because these beams can maintain a very small beam width throughout the DOF, they are also called pencil beams. Thus, when these beams are used for data transmission, the receiver can be placed at any distance within the DOF along the beam axis without degradation of received signals. Also, the signals are more difficult to be intercepted due to the narrow beam width, increasing the communication security. In addition, because these beams are pencil like, they can be stacked side by side in a two-dimensional (2D) grid to form multiple communication channels in a plane that is perpendicular to the wave propagation axis to greatly increase the data transmission rate. When a piece of information is broken up into segments, scrambled, and then transmitted over multiple channels, security is further enhanced.

This paper is organized as follows. A brief theory of the X wave and Bessel pulses will be presented, followed by both computer simulations and experiments to show the feasibility

Jian-yu Lu is with the Department of Bioengineering, The University of Toledo, Toledo, Ohio 43606, USA. (e-mail: jian-yu.lu@ieee.org).

of data transmission using single and multiple communication channels. Finally, a discussion and conclusion will be given.

## II. Theoretical Preliminaries

The scalar wave equation in free space for light and in isotropic/homogeneous media for sound in cylindrical coordinates is given by [26]:

$$\left[\frac{1}{r}\frac{\partial}{\partial r}\left(r\frac{\partial}{\partial r}\right)+\frac{1}{r^2}\frac{\partial^2}{\partial \phi^2}+\frac{\partial^2}{\partial z^2}-\frac{1}{c^2}\frac{\partial^2}{\partial t^2}\right]\Phi(r,\phi,z;t)=0\,, \quad (1)$$

where $r=\sqrt{x^2+y^2}$ is radial distance, $\phi$ is azimuthal angle, $z$ is the axial axis along which wave propagates, $t$ is time, $c$ is the speed of light in vacuum or speed of sound in isotropic/homogeneous media, and $\Phi(r,\phi,z;t)$ is the Hertz potential or acoustic pressure. To get a wave that do not change its shape as it propagates to infinite distance, it is to find a solution $\Phi(r,\phi,z;t) = \Phi(r,\phi,z-c_1t)$, where $c_1$ is a constant velocity of the wave that propagates in the $z$ direction. It is easy to prove that the following function is a solution to Eq. (1) [6]:

$$\Phi(r,\phi,z;t)=e^{in\phi}\int_0^\infty B(k)J_n(qr)e^{-ka_0+ik_z(z-c_1t)}dk\,, \quad (2)$$

where $i=\sqrt{-1}$, $n=0,1,2,\cdots$ is an integer, $k=\omega/c$ is the wave number, $\omega=2\pi f$ is the angular frequency, $f$ is the frequency, $B(k)$ is an arbitrary function (well behaved) of $k$ and can represent the transfer function of a practical transmitter system, $J_n(\cdot)$ is the $n$ th-order Bessel function of the first kind, $a_0>0$ is a real constant, $k_z=\sqrt{k^2-q^2}$ is the $z$ component of the wave number, and $c_1=\omega/k_z$. If $q=k\sin\zeta$, then $k_z=\sqrt{k^2-(k\sin\zeta)^2}=k\cos\zeta$ and $c_1=c/\cos\zeta$, where $0\le\zeta<\pi/2$ is an Axicon angle [17], we obtain an axially symmetric three-dimensional (3D) X wave [6]:

$$\Phi_{X_n}(r,\phi,z-c_1t)=e^{in\phi}\int_0^\infty B(k)J_n(kr\sin\zeta)e^{-k[a_0-i\cos\zeta(z-\frac{c}{\cos\zeta}t)]}dk\,, \quad (3)$$

where the subscript "$X_n$" denotes an nth-order X wave. If $q=\alpha$, where $0\le\alpha<k$ is a real constant for a propagating wave, and $k_z=\sqrt{k^2-\alpha^2}$, we obtain an axially symmetric 3D Bessel pulse [14-16]:

$$\Phi_{B_n}(r,\phi,z;t)=e^{in\phi}J_n(\alpha r)\int_0^\infty B(k)e^{-ka_0+ik_z(z-\frac{\omega}{k_z}t)}dk\,, \quad (4)$$

where the subscript "$B_n$" denotes an nth-order Bessel pulse. When $n=0$, both X wave and Bessel pulse are axially symmetric and have a peak at $r=0$.

Using a 2D form of Eq. (1) in rectangular coordinates (assuming the wave does not change in $y$ direction) [27]:

$$\left[\nabla^2-\frac{1}{c^2}\frac{\partial^2}{\partial t^2}\right]\Phi(\vec{r},t)=0\,, \quad (5)$$

where $\nabla^2=(\partial^2/\partial x^2+\partial^2/\partial z^2)$ is the Laplacian [27], $\vec{r}=(x,z)$ is a vector in the rectangular coordinates, one obtains a 2D X wave and Bessel pulse (also called array beams [28-29]) that can be produced by a one-dimensional (1D) linear array transducer, respectively:

$$\Phi_{X^2}(x,z-c_1t)=\int_0^\infty B(k)\cos(kx\sin\zeta)e^{ik\cos\zeta(z-\frac{c}{\cos\zeta}t)]}dk \quad (6)$$

and

$$\Phi_{B^2}(x,z;t)=\cos(\alpha x)\int_0^\infty B(k)e^{ik_z(z-\frac{\omega}{k_z}t)]}dk\,, \quad (7)$$

where the superscript in $X^2$ and $B^2$ represents 2D. Notice that unlike 3D beams, the 2D beams are not localized around the wave propagation axis unless an aperture apodization in the $x$ axis is applied, which will cause wave diffraction.

From Eq. (3) or (6), one obtains the phase $v_{pX}$ and group $v_{gX}$ velocities of the X wave:

$$v_{pX}=\frac{\omega}{k_z}=\frac{c}{\cos\zeta}\ge c \text{ and } v_{gX}=\frac{\partial\omega}{\partial k_z}=\frac{c}{\cos\zeta}\ge c\,. \quad (8)$$

From Eqs. (4) or (7), the phase $v_{pB}$ and group $v_{gB}$ velocities of the Bessel pulse can be obtained:

$$v_{pB}=\frac{\omega}{k_z}=\frac{\omega}{\sqrt{k^2-\alpha^2}}\ge c \quad (9)$$

and

$$v_{gB}=\frac{\partial\omega}{\partial k_z}=c\sqrt{1-(\frac{\alpha}{k})^2}\le c\,. \quad (10)$$

To produce the theoretical X waves (Eqs. (3) and (6)) and Bessel pulses (Eqs. (4) and (7)), a transmitter (wave source) with an infinite aperture is required. In practice, when the aperture of the wave source is finite of a radius $a$, the depth of field of the X waves and Bessel pulses respectively will be finite as follows [6]:

$$DOF_X=a\cot\zeta \quad (11)$$

and [16]

$$DOF_B=a\sqrt{(\frac{k_0}{\alpha})^2-1}\,, \quad (12)$$

where $k_0=2\pi f_0/c$ and $f_0$ is the center frequency of the pulses. As $a\to\infty$, DOF becomes infinity and both the

approximate X wave and Bessel pulse approach their theoretical limits given in Eqs. (3) and (4) respectively.

To produce a binary code such as "1011" with X wave and Bessel pulse respectively for data communications, four time-shifted versions of Eqs. (3) and (4) are superposed coherently with a fixed time interval $\Delta t$ between the digits and the amplitude of each shifted wave is multiplied by the digit (when a digit is "0", the corresponding amplitude will be 0).

## III. Computer Simulation

To show how X waves and Bessel pulses can be used to transmit binary codes such as "1011", a computer simulation was conducted. In the simulation, the speed of wave was assumed to be $c$ = 1500 m/s for ultrasound in water at the room temperature. A flat transducer with a center frequency of 2.5 MHz and a diameter of 50 mm was used. The system transfer function $B(k)$ of the transducer was assumed to be approximated with a Blackman window function [30] that has a FWHM (full-width-at-half-maximum) bandwidth of about 81% of the center frequency. The drive signal for the transducer was produced with Eq. (3) for X wave [7] and Eq. (4) for Bessel pulse [16] by setting $z = 0$ (at the transducer surface) and $n = 0$ (axially symmetric pulse) after excluding $B(k)$, and the waves were obtained at one temporal frequency a time using the method published previously [31]. For X wave, $a_0$ = 0.05 mm and $\zeta = 4°$, which give a DOF of about 357.52 mm. For Bessel pulse, $a_0$ = 0 and $\alpha = 1202.45$ m$^{-1}$, which give a DOF of about 216.28 mm at the center frequency. For a better transfer of electrical power to the transducer, a one-and-a-half-cycle 2.5-MHz sine signal was used to convolve with the drive signal [16]. The binary code was then obtained by coherently superposing the shifted versions of the X wave and Bessel pulse respectively by $\Delta t = 1.2$ $\mu$s. For comparison, both spherical wave pulses (approximately produced with a small disc transducer of about 2-mm radius) and Gaussian (25-mm FWHM Gaussian aperture weighting) pulses focused at $F$ = 170 mm and 100 mm respectively were simulated in Figs. 1 and 2. The speed of both the spherical wave pulses and the focused Gaussian pulses equals to $c$.

To increase the transmission data rate over a large depth of field for X wave and Bessel pulses, the single-channel binary code (see Figs. 1 and 2 respectively) was shifted transversely (perpendicular to the wave propagation direction) and then coherently combined with other binary codes such as "1001" and "1111" (see Figs. 3 and 4 respectively). The binary codes from multiple channels can be received by an array of receivers anywhere along the path of the beams within the large DOF with a proper setting of detection threshold. The separation between different channels that transmit binary codes was about 8.75 mm.

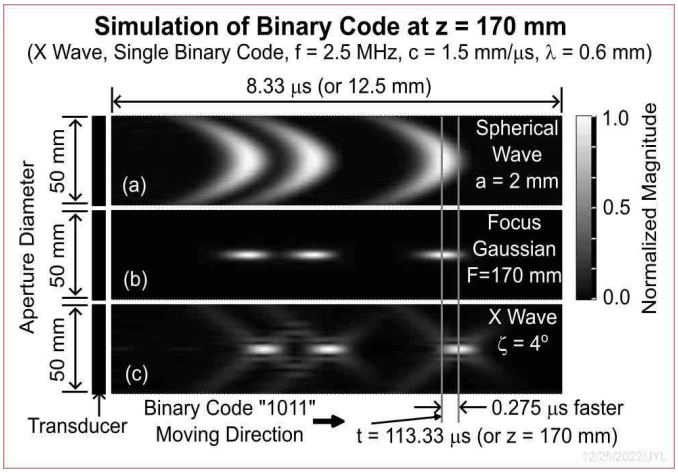


**Fig. 1.** Computer simulation of a binary code "1011" (digital information, the code is read from right to left) received at an axial distance $z$ = 170 mm away from the surface of the transducer (wave transmitter) on the left. The binary code was produced by (a) spherical wave pulses generated approximately by a small disc transmitter of about 2-mm radius, (b) Gaussian pulses with 25-mm full-width-at-half-maximum aperture apodization and focused at $F$ = 170 mm, and (c) X wave with an Axicon angle $\zeta = 4°$ and depth of field of 357.52 mm. The transducer diameter was 50 mm for both focused Gaussion pulses and X wave, and the center frequency was 2.5 MHz with a wavelength of 0.6 mm in water. The transducer was driven by a 1.5-cycle sine-wave pulse and the fractional bandwidth of the transducer was about 81% of the center frequency. The envelope of the radio-frequency pulses was used to represent the binary code and the gray-scale bar represents the normalized ultrasound pressure. In addition, the velocity of X wave is about 0.275 $\mu s$ (or 0.243%) faster (see the vertical lines) than the spherical wave and the focused Gaussian pulses that travel at the speed of sound $c$, which is very close to the theoretical value (0.244%) calculated by the group velocity formula in Eq. (8). Other parameters used in the simulation are given in the figure.

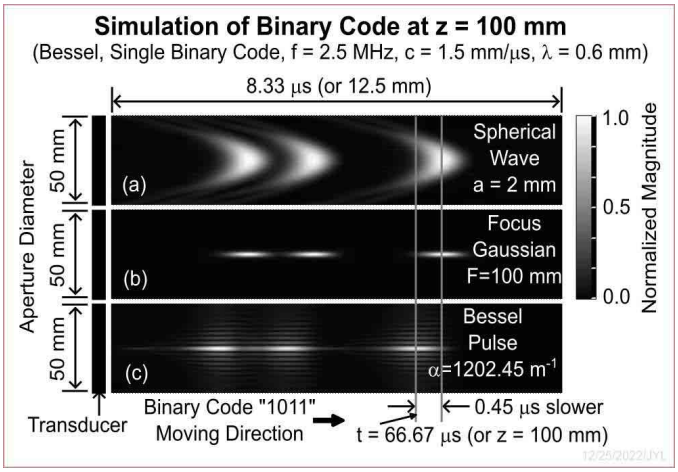


**Fig. 2.** This figure is the same as Fig. 1 except that the the binary code was received at $z$ = 100 mm, the focal lengh $F$ of the Gaussian pulses was 100 mm, and the Bessel pulses instead of X wave were used to produce the binary code. The vertical lines show that Bessel pulses with a scaling parameter $\alpha = 1202.45$ m$^{-1}$ and depth of field of 216.28 mm travel about 0.45 us (or 0.675%) slower than the spherical wave and focused Gaussian pulses that travel at the speed

of sound $c$, which is very close to the theoretical value (0.662%) calculated by Eq. (10).

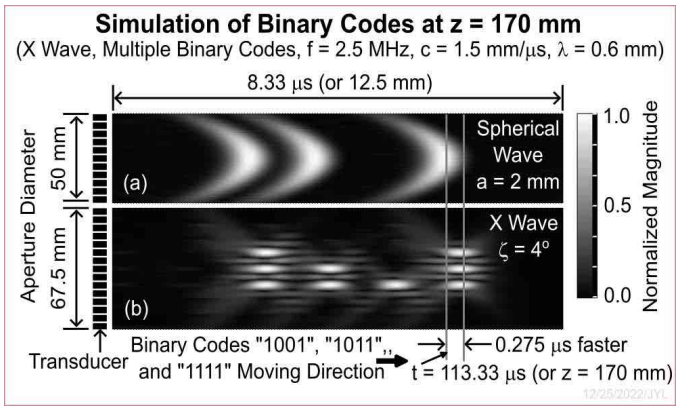


**Fig. 3.** This figure is the same as Fig. 1 except that three binary codes ("1001", "1011", and "1111") were transmitted simultaneously via three channels with a transducer of 67.5 mm x 50 mm aperture. The focused Gaussian pulses were not included since they have the same traveling velocity as the spherical wave pulses.

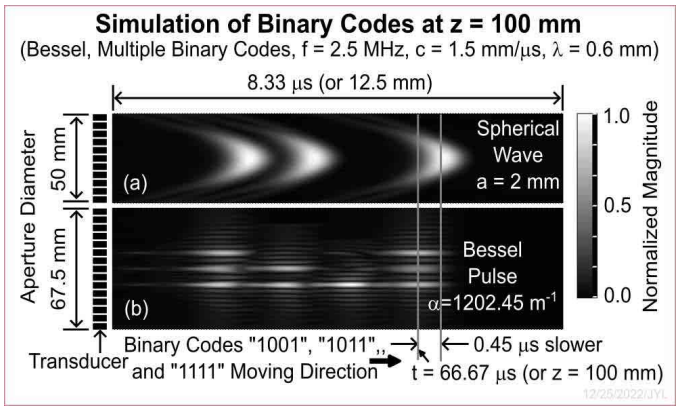


**Fig. 4.** This figure is the same as Fig. 2 except that three binary codes ("1001", "1011", and "1111") were transmitted simultaneously via three channels with a transducer of 67.5 mm x 50 mm aperture. The focused Gaussian pulses were not included since they have the same traveling velocity as the spherical wave pulses.

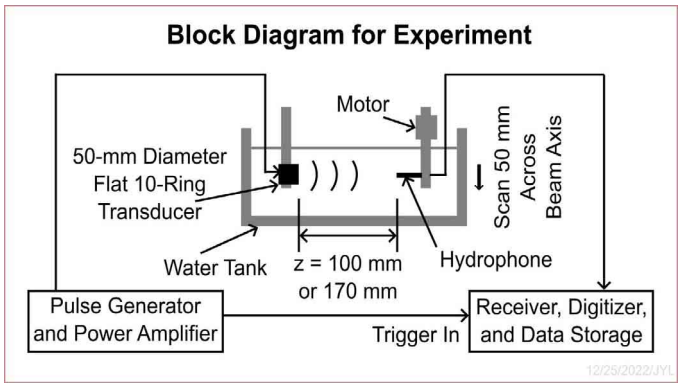


**Fig. 5.** A block diagram of experiment for measuring the binary codes (binary information) at two axial distances $z$ = 170 mm and 100 mm for X wave and Bessel pulses respectively. A flat, 2.5-MHz, about 81% fractional bandwidth, 50-mm diameter, and 10-ring annular array transducer with customized ring widths [16] was mounted on the left of a water tank. On the right, a 0.5-mm diameter and 1-20 MHz hydrophone was used to measure the sound pressure as the hydrophone scanned from top to bottom in 200 steps over 50 mm distance. In each step, an arbitrary waveform generator sent an appropriate signal via a power amplifier to each ring of the transducer, and the hydrophone received the signal after a set delay time. A digitizer (40 MS/s sampling rate) converted the received signal and stored it in a computer. This process was repeated for all 200 steps. Then, a different signal was sent to a different ring and the process was repeated until the signals from all rings were acquired and digitized. The digits of the binary code were formed by coherently supoerposing the data acquired from all rings of the transducer.

## IV. Experiment

Experiment was conducted to show that it is feasible to transmit binary codes with X wave and Bessel pulses. In the experiment, a flat, 1-3 polymer/ceramic composite, 50-mm diameter, 2.5-MHz center frequency (the bandwidth was close to that in the simulation), and 10-ring ultrasound annular array transducer was used as a transmitter [16]. The widths of the rings of the transducer were the same as those of the lobes of the Bessel function with $\alpha = 1202.45$ m$^{-1}$ [16]. Fig. 5 shows a system block diagram of the experiment. The transducer was placed on the left side of the water tank and a 0.5-mm diameter and 1-20 MHz hydrophone (NTR System, Inc.) was on the right to scan a 50-mm path vertically across the center of the wave to receive signals when each transducer ring was driven by an arbitrary waveform generator (Analogic 2045B, Analogic, Peabody, MA) and a radio-frequency power amplifier (ENI 240L, Rochester, New York). The drive signal for each transducer ring was obtained from Eq. (3) with $z = 0$ and $B(k) = 1$ for the X wave [7], and obtained using $J_0(\alpha r_i)$ in Eq. (4) combined with the one-and-a-half-cycle sine-wave electrical signal, where $r_i$ was the center radius of each ring and $i = 1, 2, \cdots, 10$ was an index of the rings, for the Bessel pulse [16]. The X wave and Bessel pulse were obtained by combining the respective signals from all 10 rings of the transducer [32]. All other parameters of the X wave and Bessel pulse were the same (including the formation of the single and multiple communication channels) as those in the simulation except that the focused Gaussian pulses were not included since their speed was the same as that of the spherical wave pulses and the Gaussian pulses have a very small depth of field.

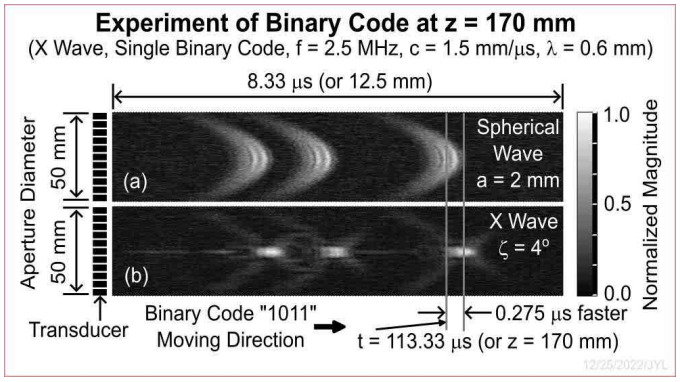


**Fig. 6.** This figure is the same as Fig. 1 except that the binary code was obtained using the experiment system in Fig. 5 and the focused Gaussian pulses were not included.

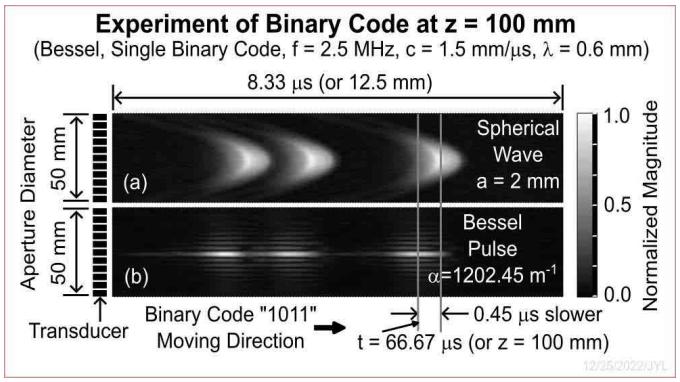


**Fig. 7.** This figure is the same as Fig. 2 except that the binary code was obtained using the experiment system in Fig. 5 and the focused Gaussian pulses were not included.

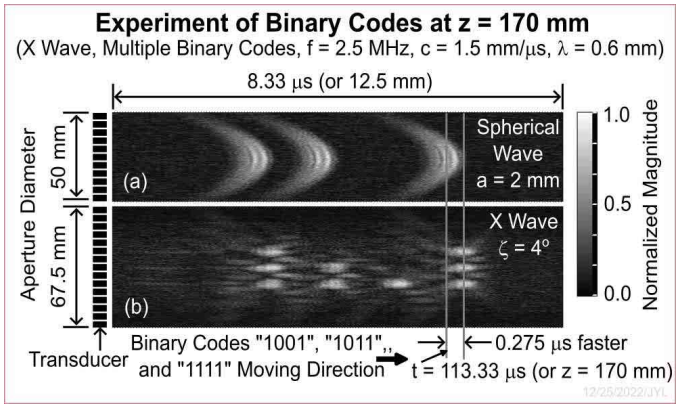


**Fig. 8.** This figure is the same as Fig. 3 except that the binary codes were obtained experimentally using the system in Fig. 5.

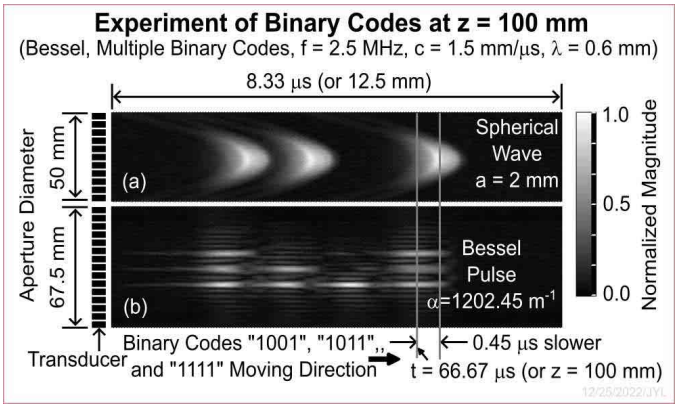


**Fig. 9.** This figure is the same as Fig. 4 except that the binary codes were obtained experimentally using the system in Fig. 5.

## V. Results

The results of the simulation of a binary code using a single channel are shown in Figs. 1 and 2 for X wave (at axial distance $z$ = 170 mm) and Bessel pulses (at $z$ = 100 mm) respectively. The results for multiple binary codes transmitted via multiple channels are given in Figs. 3 and 4 for the X wave and Bessel pulses respectively. The increased number of channels increases the data transmission rate proportionally since data can be transmitted in parallel.

The experiment results of transmitting binary codes using X wave (Figs. 6 and 8) and Bessel pulses (Figs. 7 and 9) match with the simulation results well, where each binary code was formed by superposing shifted versions of the respective X wave and Bessel pulse with $\Delta t = 1.2\ \mu s$. Different binary codes are sent via different channels that are separated 8.75 mm between the channels.

## VI. Discussion

### A. Data Transmission Rate

From both computer simulation and experiment results, it is clear that the total data transmission rate depends on the data transmission rate of each channel and the number of channels.

Data transmission rate of each channel depends on the ultrasound pulse length of each binary digit, and the pulse length depends on the center frequency and bandwidth of the ultrasound. A higher frequency allows a larger bandwidth at a given fractional bandwidth (bandwidth divided by the center frequency), and a wider bandwidth produces a shorter pulse and thus increases the data transmission rate.

Given a data transmission rate of each channel, the total data transmission rate will be proportional to the number of channels. The number of channels allowed in a given transducer aperture depends on both the center frequency and either the Axicon angle $\zeta$ of X wave (see Figs. 3 and 8) or the scaling parameter $\alpha$ of Bessel pulses (see Figs. 4 and 9). As $\zeta$ or $\alpha$ increases, the beam width becomes smaller (more localized), allowing to pack more channels into a given

transducer aperture and thus increasing the data transmission rate. However, as $\zeta$ or $\alpha$ increases, according to Eqs. (11) and (12), the depth of filed will reduce, which reduces the communication distance unless the center frequency is increased to compensate. In other words, at a given center frequency, if the communication distance is reduced, the data transmission rate can increase. In this paper, only three channels are used as an example. However, more channels can be added if the communication distance can be reduced (the DOF calculated from Eq. (11) is 357.52 mm for X wave and the DOF calculated from Eq. (12) is 216.28 mm for Bessel pulses at a center frequency of 2.5 MHz) or the frequency is increased.

The 3D X wave (Eq. (3)) and Bessel pulses (Eq. (4)) are axially symmetric when $n = 0$. Thus, channels also can be added in the direction perpendicular to those shown in Fig. 3 and 8 for X wave and Figs. 4 and 9 for Bessel pulses. If 3 channels are added in both $x$ and $y$ directions, the total number of channels will be 9. In general, if the number of channel in each direction is $N$, the total data transmission rate will be proportional to $N^2$, which can be a very big number.

### B. Wave Dispersion

Another factor that affects the data transmission rate is dispersion of the wave. From Eqs (8) to (10), it is clear that both the phase and group velocities of the X wave only depend on the Axicon angle $\zeta$, i.e., they do not depend on the temporal frequency (nondispersive). However, for Bessel pulse, both of its phase and group velocities depend not only on the scaling parameter $\alpha$, but also change with the wave number $k$ or the frequency $f$. This means that X wave pulses will not distort in the direction of propagation within their DOF while the Bessel pulses will. The dispersion makes the Bessel pulses become longer as they propagate and thus will limit the data transmission rate. This is evident from Figs. 2, 4, 7, and 9. Thus, X wave can have a higher data transmission rate than Bessel pulses. However, the electrical drive signals required to produce Bessel pulses are less complicated than those to produce X wave.

### C. Sidelobes

It is clear from Figs. 1 to 9 (except Fig. 5), both X wave and Bessel pulses have sidelobes. The sidelobes between the channels will interfere if the channels are packed too close together. Thus the sidelobes will limit the number of channels that can be packed within a give size of transducer aperture and limit the data transmission rate.

### D. Inhomogeous Media

Strictly speaking, Eq. (1) and thus its X wave solution in Eq. (3) and Bessel pulse solution in Eq. (4) are valid for isotropic/homogeneous media. In many applications, the medium is inhomogeneous and dispersive, has phase aberration, scattering, attenuation, multiple reflections, multiple paths, noise, and is even anisotropic. Depending on the severity of these distortions, the data transmission rate may be reduced.

### E. Communication Security

Data transmission with X wave or Bessel pulses allows for a more secure communication since the information is transmitted along a narrow path between the transmitter and the receiver. This makes eavesdropping more difficult since such activities are easier to be noticed by the receiver.

Using multiple channels, the eavesdropping can be even harder. This is because each channel can transmit only a part of a message, and thus getting the information from one channel may not be able to know all the information. To intercept signals from all channels, the communication may be interrupted. Also, decoding from signals received from multiple channels will be difficult without knowing how the original signals were broken up and transmitted via different channels. Beyond the DOF of X wave or Bessel pulses, diffraction makes information from all channels scrambled and thus the information may not be very useful. Also, beyond the DOF, beam intensity may become too small to be detected due to diffraction.

### F. System Complexity

To produce X wave and Bessel pulse, Eqs. (3) and (4) need to be used respectively to drive the transducer, as described in the Experiment section above. Digital codes to be transmitted can then be used to modulate the drive signals. For $n = 0$, the waves are axially symmetric and thus both the X wave and Bessel pulses can be produced with an annular array transducer with only a few elements (rings). For the parameters $\alpha$ and $\zeta$ chosen in this paper, 10 rings were enough for single-channel data transmissions.

For multiple-channel data transmission, since the X wave and Bessel pulses need to be shifted in both $x$ and $y$ directions, the resulting waves may not be axially symmetric. In this case, 2D array transducer may be needed. Although the number of elements of the 2D array can be optimized for given $\alpha$ and $\zeta$, it can be much larger than that of the annular array. Thus, the data transmission rate of multiple channels is increased at the expense of the increased system complexity.

### G. Conventional Focused Waves

Using conventional focused waves such as the focused Gaussian pulses in Figs. 1 and 2, single and multiple channel communications can be achieved in a way similar to those with the X wave and Bessel pulses. However, since the DOF of focused waves are short, detectors need to be placed at the focal distance to get the signals.

### H. Coded Excitation for Ultrasound Imaging

Using single or multiple channels, X wave and Bessel pulses can be used for pulse-echo imaging over a large DOF with coded excitations to increase signal-to-noise ratio [33]. Using multiple channels, image frame rate can be increased.

### I. Phase and Group Velocities and Delay Lines

It is clear from Eq. (8) that both the phase and group velocities of X wave are nondispersive (independent of

temporal frequency) and are larger than or equal to $c$, where $c$ is given in Eq. (1) and is the propagation speed of the spherical wave and the focused Gaussian pulse (see Figs 1, 3, 6, and 8). For Bessel pulse, both the phase (Eq. (9)) and group (Eq. (10)) velocities are dispersive, and the group velocity is always smaller than or equal to $c$ (see Figs. 2, 4, 7, and 9) and the group velocity decreases as $\alpha$ increases. From Figs. 1, 3, 6, and 8, it is seen that the traveling speed of the binary codes is about 0.275/113.33 = 0.243% faster than $c$ for X wave, which is very close to the theoretical value (0.244%) of the group velocity calculated with Eq. (8). For the Bessel pulses in Figs. 2, 4, 7, and 9, the velocity is about 0.45/66.67 = 0.675% slower than $c$, which also is very close to the theoretical value (0.662%) calculated with the group velocity formula Eq. (10).

Because the group velocity of Bessel pulses is slower than $c$ and decreases as $\alpha$ increases, the Bessel pulses can be used for delay lines. Currently, acoustic delay lines are made of surface acoustic wave (SAW) devices [34-36]. The advantage of using Bessel pulses versus SAW is that the delay time can be easily changed with $\alpha$. Also, as shown in Figs. 4 and 9, multiple channels can be packed within a given transducer aperture to increase the data transmission rate. In addition, since the Bessel pulses have a very large DOF, the delay time can be changed by simply changing the distance between the transmitter and the receiver (this is the case for X wave too). However, as mentioned before, the dispersion of Bessel pulses will limit the data transmission rate as the propagation distance increases. For X wave, there will be no dispersion.

### J. Optical and Electromagetic Waves

Because the wave equation in Eqs. (1) and (4) are the same for both light in vacuum (see X wave produced in optics [1-5], where each component of the vector electrical field and magnetic field in free space satisfies Eqs. (1) and (4)) and sound in isotropic/homogenous media, the results in Figs. 1 to 9 (except Fig. 5) are the same for light or other electromagnetic waves except that the parameters of the waves are different and $c$ is the speed of light in vacuum [11][37-38]. This means that the data communication method developed for ultrasound here can be extended to optical and other electromagnetic waves.

Notice that unlike the optical fiber communications [39], X wave communications are nondispersive and thus it may allow a higher data transmission rate. Also, Bessel pulses can be used as optical delay lines [40].

### K. More on the Velocity of the Waves

From the results in this study, it is evident that the binary code information carried by the X wave and Bessel pulses can respectively travel at a velocity that is faster or slower than the speed, $c$, of sound in isotropic/homogeneous media or the light in vacuum along the wave axis where the waves are highly localized (the transverse width of the pulses can be close to the diffraction limit of the focused Gaussian pulse at its focus, see Figs. 1 and 2), and the information can be detected by setting a proper threshold of a detector to exclude sidelobes.

The reason why X wave in Eq. (3) has a group velocity that is larger than $c$ can be explained as follows. For an arbitrary wave $\Phi(\vec{r};t)$ that is a solution to a linear wave equation, where $\vec{r}=(x,y,z)$ is a point in space, at a fixed $\vec{r}$ the wave can be expanded using the following 1D Fourier transform pair (assuming that the transformations exist) [41]:

$$\tilde{\Phi}(\vec{r};\omega)=\Im_t\{\Phi(\vec{r};t)\}=\int_{-\infty}^{\infty}\Phi(\vec{r};t)e^{i\omega t}dt\,, \tag{13}$$

and

$$\Phi(\vec{r};t)=\Im_\omega^{-1}\{\tilde{\Phi}(\vec{r};\omega)\}=\frac{1}{2\pi}\int_{-\infty}^{\infty}\tilde{\Phi}(\vec{r};\omega)e^{-i\omega t}d\omega\,, \tag{14}$$

where $\tilde{\Phi}(\vec{r};\omega)$ is the temporal Fourier transform of $\Phi(\vec{r};t)$, $\omega$ is an angular frequency, and $\Im_t\{\cdot\}$ and $\Im_\omega^{-1}\{\cdot\}$ denote the forward and inverse Fourier transforms respectively. Similarly, for each fixed $\omega$, $\tilde{\Phi}(\vec{r};\omega)$ satisfies the following 3D spatial Fourier transform pair (also assuming that the transformations exist) [41]:

$$\bar{\tilde{\Phi}}(\vec{k};\omega)=\Im_{\vec{r}}\{\tilde{\Phi}(\vec{r};\omega)\}=\int_{\vec{r}}\tilde{\Phi}(\vec{r};\omega)e^{-i\vec{k}\cdot\vec{r}}d\vec{r}\,, \tag{15}$$

and

$$\tilde{\Phi}(\vec{r};\omega)=\Im_{\vec{k}}^{-1}\{\bar{\tilde{\Phi}}(\vec{k};\omega)\}=\frac{1}{(2\pi)^3}\int_{\vec{k}}\bar{\tilde{\Phi}}(\vec{k};\omega)e^{i\vec{k}\cdot\vec{r}}d\vec{k}\,, \tag{16}$$

where $\vec{k}=(k_x,k_y,k_z)$. Inserting Eq. (16) into Eq. (14), we have:

$$\begin{aligned}\Phi(\vec{r};t)&=\frac{1}{2\pi}\int_{-\infty}^{\infty}\left[\frac{1}{(2\pi)^3}\int_{\vec{k}}\bar{\tilde{\Phi}}(\vec{k};\omega)e^{i\vec{k}\cdot\vec{r}}d\vec{k}\right]e^{-i\omega t}d\omega\\&=\frac{1}{(2\pi)^4}\int_{-\infty}^{\infty}\left[\int_{\vec{k}}\bar{\tilde{\Phi}}(\vec{k};\omega)e^{i(\vec{k}\cdot\vec{r}-\omega t)}d\vec{k}\right]d\omega\end{aligned}\,. \tag{17}$$

Eq. (17) indicates that $\Phi(\vec{r};t)$ is a linear superposition of the plane wave $e^{i(\vec{k}\cdot\vec{r}-\omega t)}$ propagating at the speed $\omega/k$ in the direction of the vector wave number $\vec{k}$ with $(1/(2\pi)^4)\bar{\tilde{\Phi}}(\vec{k};\omega)$ as its complex amplitude calculated with both Eqs. (13) and (15), where $k=|\vec{k}|=\sqrt{k_x^2+k_y^2+k_z^2}$. Inserting the plane wave above into the wave equation in Eq. (1), for the plane wave to be a solution, we must have $\omega/k=c$, i.e., the plane wave must travel at a fixed speed $c$ in the direction of $\vec{k}$. Since the X wave (see Eq. (3)) that travels in the $z$ direction is also a solution to Eq. (1), it can be expressed as a linear superposition of the plane waves that travel at speed $c$ [6]. This shows that it is the interference of these plane waves that makes the phase and group velocities of the X wave larger than or equal to $c$.

### L. deBroglie Waves

In addition to electromagnetic waves, X wave can exist in deBroglie waves [8-11,38,42]. The relativistic free-particle Klein-Gordon, Dirac, and Weyl equations all have plane wave

solutions [42], $\Phi_P(\vec{r};t)=N(p)u(\vec{p})e^{i(\vec{p}\cdot\vec{r}-Et)/\hbar}$, where $\Phi_P(\vec{r};t)$ is the wave function and the subscript "$P$" means plane wave, $\vec{r}=(x,y,z)$ is a point in space, $t$ is the time, $N(p)$ is a normalization function, $u(\vec{p})$ depends on the wave-equations, $\vec{p}=\hbar\vec{k}=(p_x,p_y,p_z)$ is a momentum vector of the particle with $p_x$, $p_y$, and $p_z$ as its components, $\vec{k}=(k_x,k_y,k_z)$ is a vector wave number with components $k_x$, $k_y$, and $k_z$, $p=\mid\vec{p}\mid=\hbar k=\gamma m_0 v_g=h/\lambda$ is the deBroglie relation, $k=\mid\vec{k}\mid=\sqrt{k_x^2+k_y^2+k_z^2}$, $\gamma=1/\sqrt{1-(v_g/c)^2}$, $m_0$ is the rest mass (for some particles such as photon and neutrino, $m_0=0$), $c$ here is the speed of light in vacuum, $h$ is the Plank's constant, $\hbar=h/(2\pi)$ is the reduced Plank's constant, $E=\pm E^+$ (the "+" and "-" signs before $E^+$ are for particles and antiparticles respectively) and $E^+=\mid E\mid=\gamma m_0c^2=hf=\hbar\omega$, (also $E^{+2}=p^2c^2+m_0^2c^4$) is the total energy of the particle [43], $f$ is the frequency of the wave, $\omega=2\pi f$ is the angular frequency, $\lambda$ is the wavelength, $v_g=\partial E^+/\partial p\le c$ is the group velocity of the plane wave or the speed of the free particle in the direction of $\vec{p}$, and $v_p=E^+/p=\gamma m_0c^2/(\gamma m_0v_g)=f\lambda=c^2/v_g\ge c$ is the phase velocity of the plane wave, which is much larger than $c$ for a small $v_g$ due to a large wavelength $\lambda$.

Let $k_x=k\sin\zeta\cos\theta$, $k_y=k\sin\zeta\sin\theta$, $k_z=k\cos\zeta$, $x=r\cos\phi$, $y=r\sin\phi$, where $r=\sqrt{x^2+y^2}$ is the radial distance and $0\le\phi<2\pi$ is the polar angle in the $x-y$ plane, $0\le\theta<2\pi$ is the polar angle in the $k_x-k_y$ plane, and $0\le\zeta<\pi/2$ is an Axicon angle [17], superposing the plane wave over the free parameters $\theta$ and $k$, noticing that $e^{i(\vec{p}\cdot\vec{r}-Et)/\hbar}=e^{i(\vec{k}\cdot\vec{r}\mp\omega t)}=e^{i(k_xx+k_yy)+i(k_z z\mp\omega t)}$, and using the procedure in Eqs (2), (5), (6), and (12) of [6], one obtains the X wave solutions to the free-particle Klein-Gordon, Dirac, and Weyl equations:

$$\Phi_{X_n}(\vec{r};t)=\int_{k_{\min}}^{k_{\max}}B(k)e^{-a_0k}\left[\frac{(-i)^n}{2\pi}\int_{-\pi}^{\pi}e^{in\theta}u(\vec{p})e^{i(\vec{k}\cdot\vec{r}\mp\omega t)}d\theta\right]dk$$
$$=\int_{k_{\min}}^{k_{\max}}B(k)\left[\frac{(-i)^n}{2\pi}\int_{-\pi}^{\pi}u(\vec{p})e^{in\theta}e^{i(k\sin\zeta)r\cos(\phi-\theta)}d\theta\right]e^{-k[a_0-i\cos\zeta(z\mp c_1t)]}dk, \quad (18)$$

where $i=\sqrt{-1}$, $n=0,1,2,\cdots$ is an integer, $B(k)$ is an arbitrary function (well behaved) of $k$ (including the normalization function $N(p)=N(\hbar k)$), $a_0>0$ is a real constant, $c_1=v_p/\cos\zeta$ is a real constant velocity of the X wave propagating in the $z$ direction (or $\zeta=\cos^{-1}(v_p/c_1)$ with $v_p/c_1=(c^2/v_g)/c_1\le1$ and $c^2/c_1=v_{g_{\min}}\le v_g\le v_{g_{\max}}\le c$), $k_{\min}=m_0c/(\hbar\sqrt{(c_1/c)^2-1})$, and $k_{\max}=m_0c/(\hbar\sqrt{(c/v_{g_{\max}})^2-1})$ (notice that $k$ and $v_g$ are related by $k=p/\hbar=\gamma m_0v_g/\hbar$ or $k=m_0c/(\hbar\sqrt{(c/v_g)^2-1})$ if $v_g\ne c$), where $v_{g_{\min}}=c^2/c_1$ and $v_{g_{\max}}$ are real constants. If $c_1\to\infty$, then $k_{\min}\to0$, and if $v_{g_{\max}}\to c$, we have $k_{\max}\to\infty$. For massless particles ($m_0=0$, $v_p=v_g=c$, and $E^+=\hbar\omega=pc$), we have $k=p/\hbar=(\hbar\omega/c)/\hbar=\omega/c$ with $k_{\min}=0$ (when $\omega=0$) and $k_{\max}=\infty$ (when $\omega\to\infty$), which is consistent with the X wave in Eq. (3).

For the free Klein-Gordon equation (massive spin-0 particles) [42]:

$$\left[\nabla^2-\frac{1}{c^2}\frac{\partial^2}{\partial t^2}-\frac{m_0^2c^2}{\hbar^2}\right]\Phi(\vec{r},t)=0, \quad (19)$$

where $\nabla^2=\partial^2/\partial x^2+\partial^2/\partial y^2+\partial^2/\partial z^2$ is the Laplacian, and, $u(\vec{p})=1$ in Eq. (18). Using the identity of Bessel function [44]:

$$J_n(kr\sin\zeta)e^{in\phi}=\frac{(-i)^n}{2\pi}\int_{-\pi}^{\pi}e^{in\theta}e^{ikr\sin\zeta\cos(\phi-\theta)}d\theta, \quad (20)$$

where $J_n(\cdot)$ is the $n$ th-order Bessel function of the first kind, we obtain the X wave solution from Eq. (18):

$$\Phi_{X_n}(\vec{r};t)=e^{in\phi}\int_{k_{\min}}^{k_{\max}}B(k)J_n(kr\sin\zeta)e^{-k[a_0-i\cos\zeta(z\mp c_1t)]}dk, \quad (21)$$

which is the same as Eq. (3) of the wave equation in Eq. (1), except that $\zeta$ now depends on $v_p=c^2/v_g$ or the momentum $p=\gamma m_0v_g=\hbar k$ of the particle and the integration of $k$ starts from $k_{\min}$ to $k_{\max}$. Notice that for the free Klein-Gordon equation, the plane wave can have both positive and negative energy $E=\pm\hbar\omega$, and the positive and negative $E$ represent particles and antiparticles respectively [42].

For the free Dirac equation (massive spin-1/2 particles) [42]:

$$\begin{cases}i\hbar\dfrac{\partial\Phi_1}{\partial t}=\dfrac{\hbar c}{i}\left(\dfrac{\partial\Phi_4}{\partial x}-i\dfrac{\partial\Phi_4}{\partial y}+\dfrac{\partial\Phi_3}{\partial z}\right)+m_0c^2\Phi_1\\ i\hbar\dfrac{\partial\Phi_2}{\partial t}=\dfrac{\hbar c}{i}\left(\dfrac{\partial\Phi_3}{\partial x}+i\dfrac{\partial\Phi_3}{\partial y}-\dfrac{\partial\Phi_4}{\partial z}\right)+m_0c^2\Phi_2\\ i\hbar\dfrac{\partial\Phi_3}{\partial t}=\dfrac{\hbar c}{i}\left(\dfrac{\partial\Phi_2}{\partial x}-i\dfrac{\partial\Phi_2}{\partial y}+\dfrac{\partial\Phi_1}{\partial z}\right)-m_0c^2\Phi_3\\ i\hbar\dfrac{\partial\Phi_4}{\partial t}=\dfrac{\hbar c}{i}\left(\dfrac{\partial\Phi_1}{\partial x}+i\dfrac{\partial\Phi_1}{\partial y}-\dfrac{\partial\Phi_2}{\partial z}\right)-m_0c^2\Phi_4\end{cases}, \quad (22)$$

where $\Phi_1$, $\Phi_2$, $\Phi_3$, and $\Phi_4$ are the four components of the wave function array $\Phi(\vec{r},t)=[\Phi_1,\Phi_2,\Phi_3,\Phi_4]^T$, and the

superscript " $T$ " means transpose, $u(\vec{p})$ in the plane wave solution to Eq. (22) consists of four independent arrays and each array contains four components as follows [42]:

$$u^{(1)}(\vec{p})=\begin{bmatrix}1\\0\\\frac{pc\cos\zeta}{E+m_0c^2}\\\frac{pc\sin\zeta}{E+m_0c^2}e^{i\theta}\end{bmatrix},\ u^{(2)}(\vec{p})=\begin{bmatrix}0\\1\\\frac{pc\sin\zeta}{E+m_0c^2}e^{-i\theta}\\\frac{-pc\cos\zeta}{E+m_0c^2}\end{bmatrix}$$

$$u^{(3)}(\vec{p})=\begin{bmatrix}\frac{-pc\cos\zeta}{-E+m_0c^2}\\\frac{-pc\sin\zeta}{-E+m_0c^2}e^{i\theta}\\1\\0\end{bmatrix},\ u^{(4)}(\vec{p})=\begin{bmatrix}\frac{-pc\sin\zeta}{-E+m_0c^2}e^{-i\theta}\\\frac{pc\cos\zeta}{-E+m_0c^2}\\0\\1\end{bmatrix},\quad(23)$$

where the arrays $u^{(1)}(\vec{p})$ and $u^{(2)}(\vec{p})$ correspond to $E>0$ (particles), and the arrays $u^{(3)}(\vec{p})$ and $u^{(4)}(\vec{p})$ are for $E<0$ (antiparticles) [42]. The X wave array $\Phi_{X_n}(\vec{r};t)$ in Eq. (18), which is a solution to Eq. (22), also has four components for each of $u^{(j)}(\vec{p})$, where $j=1,2,3,4$, and the four solutions $\Phi^{(j)}_{X_n}(\vec{r};t)$ that correspond to the four independent arrays $u^{(j)}(\vec{p})$ in Eq. (23) can be obtained from Eq. (18) and be used to construct other X-wave solutions through a linear combination. For the components of $u^{(j)}(\vec{p})$ that contain $e^{i\theta}$ and $e^{-i\theta}$, the corresponding components of $\Phi^{(j)}_{X_n}(\vec{r};t)$ should be divided and multiplied by $-i$, and have their order $n$ increased and decreased by 1, respectively (see Eqs. (18) and (20)).

For the free Weyl equations (massless, i.e., $m_0=0$, spin-1/2 particles) with right- and left-handed screw forms (refer to the spin in the direction of momentum $\vec{p}$) respectively [42]:

$$i\hbar\frac{\partial}{\partial t}\begin{bmatrix}\Phi_1^R\\\Phi_2^R\end{bmatrix}=\frac{\hbar c}{i}\left\{\frac{\partial}{\partial x}\begin{bmatrix}\Phi_2^R\\\Phi_1^R\end{bmatrix}+i\frac{\partial}{\partial y}\begin{bmatrix}-\Phi_2^R\\+\Phi_1^R\end{bmatrix}+\frac{\partial}{\partial z}\begin{bmatrix}+\Phi_1^R\\-\Phi_2^R\end{bmatrix}\right\}\quad(24)$$

and

$$i\hbar\frac{\partial}{\partial t}\begin{bmatrix}\Phi_1^L\\\Phi_2^L\end{bmatrix}=-\frac{\hbar c}{i}\left\{\frac{\partial}{\partial x}\begin{bmatrix}\Phi_2^L\\\Phi_1^L\end{bmatrix}+i\frac{\partial}{\partial y}\begin{bmatrix}-\Phi_2^L\\+\Phi_1^L\end{bmatrix}+\frac{\partial}{\partial z}\begin{bmatrix}+\Phi_1^L\\-\Phi_2^L\end{bmatrix}\right\},\quad(25)$$

where $\Phi^R(\vec{r},t)=[\Phi_1^R,\Phi_2^R]^T$ and $\Phi^L(\vec{r},t)=[\Phi_1^L,\Phi_2^L]^T$ are wave function arrays of Eqs (24) and (25) respectively, the superscripts $R$ and $L$ represent "right handed" and "left handed" respectively, $u(\vec{p})$ is given by: [42]:

$$u^R(\vec{p})=\begin{bmatrix}\cos(\zeta/2)\\\sin(\zeta/2)e^{i\theta}\end{bmatrix}\text{ and }u^L(\vec{p})=\begin{bmatrix}\sin(\zeta/2)\\-\cos(\zeta/2)e^{i\theta}\end{bmatrix},\quad(26)$$

where $u^R(\vec{p})$ and $u^L(\vec{p})$ are related to the plane-wave solutions of Eqs. (24) and (25) respectively [42]. When both the free right- and left-handed Weyl equations are used, only $E>0$ needs to be considered since one equation represents particles and the other represents antiparticles [42]. In this case, the "$\mp$" in Eq. (18) should take the "$-$" sign only. Also, for the $u(\vec{p})$ components that contain $e^{i\theta}$, the corresponding components of the X wave solutions $\Phi_{X_n}(\vec{r};t)$ (see Eq. (18)) to Eqs. (24) and (25) should be divided by $-i$ and have their order $n$ increased by 1 (see Eqs. (18) and (20)). Because Weyl equations describe massless spin-1/2 particles, $v_g=v_p=c$ and $c_1=c/\cos\zeta$, their X wave solutions in Eq. (18) have the same $v_g$ and $c_1$ as those of the X wave in Eq. (3).

From Eq. (18), it is clear that the phase and group velocities of the X wave (propagating in the $z$ direction) are given by $v_{pX}=E^+/p_z=(p_zc_1)/p_z=c_1$ and $v_{gX}=\partial E^+/\partial p_z=\partial(p_zc_1)/\partial p_z=c_1$ respectively, where $c_1\geq c$ is a constant. This means that X wave is nondispersive and can propagate rigidly at velocity $c_1$. For a free particle that travels at a fixed speed $v_g$ in the direction of $\vec{p}$, according to the uncertainty principle, it can appear in any place in the space $\vec{r}$, as is described by its associated plane wave [45]. Also the plane wave can have a finite time duration as is seen in this study (see Figs 1-9 except 5), this means that the energy $E^+=\hbar\omega=\hbar kv_p$ of the particles has a spread [45]. When the plane waves of these particles are superposed coherently, the particles can cluster together near the peak of the X wave (Eq. (18)) that moves rigidly at a constant velocity $c_1\geq c$ (notice that $|\Phi_{X_n}(\vec{r};t)|^2=\Phi^H_{X_n}(\vec{r};t)\Phi_{X_n}(\vec{r};t)$, where the superscript "$H$" represents the Hermitian conjugate and $\Phi_{X_n}(\vec{r};t)$ is an array of multiple components, is the probability density of finding a particle at position $\vec{r}$ and time $t$ for the Dirac and Weyl equations, and $\Phi_{X_n}(\vec{r};t)$ is a scalar that is related to the charge density for the Klein-Gordon equation [42]). This is consistent with what observed in the quantum entanglement experiments in which the quantum mechanics follows the superposition and statistical rules governed by the wave functions [46-48], instead of following a deterministic rule with "hidden variables" [49]. Also, X wave can be used as orthogonal bases to construct other waves of linear wave equations through an X wave transform [50].

## VII. Conclusion

X wave and Bessel pulses are used to transmit binary data information in a highly localized space over a large depth of field (DOF) in ultrasound. The large DOF makes it easier for detector placement since signals can be received at any distance along the beam path within the DOF. Because both X wave and Bessel pulses are highly localized around the beam

axis, multiple communication channels can be formed to transmit signals in parallel to greatly increase the data transmission rate and communication security. Also, because Bessel pulses have a lower group velocity, they can be used as a delay line.

Since the wave equation in Eq. (1) is the same for both sound and light, the study here in ultrasound is also applicable to optical and other electromagnetic waves if the relevant parameters are changed properly in the respective fields [11][37-38]. In addition, because free-particle Klein-Gordon, Dirac, and Weyl equations [42] all have X wave solutions, the ultrasound X wave studied here is relevant to the deBroglie wave in quantum mechanics.

## REFERENCES


[1] H. Kondakci and A. F. Abouraddy. "Optical space-time wave packets having arbitrary group velocities in free space." *Nature Communications* 10, no. 1 (2019): 1-8.

[2] H. Kondakci and A. F. Abouraddy. "Diffraction-free space–time light sheets." *Nature Photonics* 11, no. 11 (2017): 733-740.

[3] C. Guo, M. Xiao, M. Orenstein, and S. Fan. "Structured 3D linear space–time light bullets by nonlocal nanophotonics." *Light: Science & Applications* 10, no. 1 (2021): 1-15.

[4] P. Saari. "Reexamination of group velocities of structured light pulses." *Physical Review A* 97, no. 6 (2018): 063824.

[5] P. Saari and K. Reivelt. "Evidence of X-shaped propagation-invariant localized light waves." *Physical Review Letters* 79, no. 21 (1997): 4135.

[6] Jian-yu Lu and J. F. Greenleaf. "Nondiffracting X waves-exact solutions to free-space scalar wave equation and their finite aperture realizations." *IEEE Transactions on Ultrasonics, Ferroelectrics, and Frequency Control* 39, no. 1 (1992): 19-31.

[7] Jian-yu Lu and J. F. Greenleaf. "Experimental verification of nondiffracting X waves." *IEEE Transactions on Ultrasonics, Ferroelectrics, and Frequency Control* 39, no. 3 (1992): 441-446.

[8] Waldyr A. Rodrigues and Jian-yu Lu. "On the existence of undistorted progressive waves (UPWs) of arbitrary speeds $0 \leq \vartheta < \infty$ in nature." *Foundations of Physics* 27, no. 3 (1997): 435-508.

[9] L. Mackinnon, "A nondispersive de Broglie wave packet." *Foundations of Physics* 8, no. 3 (1978): 157-176.

[10] A. M. Shaarawi, I. M. Besieris, and R. W. Ziolkowski. "A novel approach to the synthesis of nondispersive wave packet solutions to the Klein–Gordon and Dirac equations." *Journal of Mathematical Physics* 31, no. 10 (1990): 2511-2519.

[11] Jian-yu Lu, J. F. Greenleaf, and E. Recami. "Limited-Diffraction Solutions to Maxwell and to Schroedinger Equations." *arXiv preprint physics/9610012* (1996).

[12] J. N. Brittingham, "Focus waves modes in homogeneous Maxwell's equations: Transverse electric mode." *Journal of Applied Physics* 54, no. 3 (1983): 1179-1189.

[13] R. W. Ziolkowski, "Exact solutions of the wave equation with complex source locations." *Journal of Mathematical Physics* 26, no. 4 (1985): 861-863.

[14] J. A. Stratton. *Electromagnetic theory*. Mcgrow-Hill Book Company, Inc, New York, and London (1941): 205-207. Page 356.

[15] J. Durnin, "Exact solutions for nondiffracting beams. I. The scalar theory." *JOSA A* 4, no. 4 (1987): 651-654.

[16] Jian-yu Lu and J. F. Greenleaf. "Ultrasonic nondiffracting transducer for medical imaging." *IEEE Transactions on Ultrasonics, Ferroelectrics, and Frequency Control* 37, no. 5 (1990): 438-447.

[17] J. H. McLeod. "The axicon: a new type of optical element." *JOSA* 44, no. 8 (1954): 592-597.

[18] Jian-yu Lu, H. Zou, and J. F. Greenleaf. "Biomedical ultrasound beam forming." *Ultrasound in medicine & biology* 20, no. 5 (1994): 403-428.

[19] Jian-yu Lu. "2D and 3D high frame rate imaging with limited diffraction beams." *IEEE Transactions on Ultrasonics, Ferroelectrics, and Frequency Control* 44, no. 4 (1997): 839-856.

[20] C. M. G. Gussen, P. S. R. Diniz, M. L. R. Campos, W. A. Martins, F. M. Costa, and J. N. Gois. "A survey of underwater wireless communication technologies." *J. Commun. Inf. Sys* 31, no. 1 (2016): 242-255.

[21] B. Szlachetko. "Low-Cost Underwater Communication System: A Pilot Study." *Applied Sciences* 12, no. 7 (2022): 3287.

[22] D.-X. Yang, Z. Hu, H. Zhao, H.-F. Hu, Y.-Z. Sun, and B.-J. Hou. "Through-metal-wall power delivery and data transmission for enclosed sensors: A review." *Sensors* 15, no. 12 (2015): 31581-31605.

[23] J. Zhang, Z. Yu, H. Yang, M. Wu, and J. Yang. "Wireless communication using ultrasound through metal barriers: Experiment and analysis." In *2015 10th International Conference on Information, Communications and Signal Processing (ICICS)*, pp. 1-5. IEEE, 2015.

[24] Z. Kou, R. J. Miller, A. C. Singer, and M. L. Oelze. "High data rate communications in vivo using ultrasound." *IEEE Transactions on Biomedical Engineering* 68, no. 11 (2021): 3308-3316.

[25] B. Herrera, E. Demirors, G. Chen, R. Guida, F. Pop, N. Dave, C. Cassella, T. Melodia, and M. Rinaldi. "Pmut-based high data rate ultrasonic wireless communication link for intra-body networks." In *Proc. Hilton Head MEMS Workshop*, pp. 1-4. 2017.

[26] F. John. *Partial Differential Equations*. New York: Springer-Verlag, 1982.

[27] J. W. Goodman. *Introduction to Fourier Optics*. New York McGraw-Hill (1968). Chs. 2-4.

[28] Jian-yu Lu. "Limited diffraction array beams." *International journal of imaging systems and technology* 8, no. 1 (1997): 126-136.

[29] Jian-yu Lu, J. Cheng, and J. Wang. " High frame rate imaging system for limited diffraction array beam imaging with square-wave aperture weightings." *IEEE Transactions on Ultrasonics, Ferroelectrics, and Frequency Control* 53, no. 10 (2006): 1796-1812.

[30] A. V. Oppenheim, and R. W. Schafer. *Digital signal processing*. *Englewood Cliffs, N. J., Prentice-Hall, Inc., 1975. 598p* (1975). Ch. 5.

[31] Jian-yu Lu and J. Cheng. "Field computation for two-dimensional array transducers with limited diffraction array beams." *Ultrasonic Imaging* 27, no. 4 (2005): 237-255.

[32] Jian-yu Lu and J. F. Greenleaf. "Formation and propagation of limited diffraction beams." In *Acoustical Imaging*, pp. 331-343. Springer, Boston, MA, 1993.

[33] T. X. Misaridis, K. Gammelmark, C. H. Jørgensen, N. Lindberg, A. H. Thomsen, M. H. Pedersen, and J. A. Jensen. "Potential of coded excitation in medical ultrasound imaging." *Ultrasonics* 38, no. 1-8 (2000): 183-189.

[34] L. M. Reindl, and C. .Ruppel. "Surface Acoustic Wave Delay Lines." *Encyclopedia of RF and Microwave Engineering* (2005).

[35] C. Gruber, A. Binder, and M. Lenzhofer. "Fast phase analysis of SAW delay lines." In *International Internet of Things Summit*, pp. 373-382. Springer, Cham, 2015.

[36] R. M. Hays and C. S. Hartmann. "Surface-acoustic-wave devices for communications." *Proceedings of the IEEE* 64, no. 5 (1976): 652-671.

[37] Jian-yu Lu and S. He. "Optical X wave communications." *Optics Communications* 161, no. 4-6 (1999): 187-192.

[38] Lu, Jian-Yu. "Ultrasonic Imaging with Limited-Diffraction Beams." *Localized Waves* (2008): 97-128. (Also in arXiv.org:physics/0603190.)

[39] S. H. Wemple. "Material dispersion in optical fibers." *Applied Optics* 18, no. 1 (1979): 31-35.

[40] S. Khan, M. A. Baghban, and S. Fathpour. "Electronically tunable silicon photonic delay lines." *Optics Express* 19, no. 12 (2011): 11780-11785.

[41] R. N. Bracewell. *The Fourier transform and its applications*. Vol. 31999. New York: McGraw-Hill, 1986.

[42] W. Greiner. *Relativistic quantum mechanics*. Vol. 2. springer, Berlin, 2000.

[43] A. Einstein. "On the electrodynamics of moving bodies." *Annalen der Physik* 17, no. 10 (1905): 891-921.

[44] I. S. Gradshteyn and I. M. Ryzhik. *Table of integrals, series, and products*. D. Zwillinger and A. Jeffrey, Eds, Academic press, 2007. P. 912.

[45] P. Busch, T. Heinonen, and P. Lahti. "Heisenberg's uncertainty principle." *Physics Reports* 452, no. 6 (2007): 155-176.

[46] S. J. Freedman and J. F. Clauser. "Experimental test of local hidden-variable theories." *Physical Review Letters* 28, no. 14 (1972): 938.

[47] A. Aspect, P. Grangier, and G. Roger. "Experimental realization of Einstein-Podolsky-Rosen-Bohm Gedankenexperiment: a new violation of Bell's inequalities." *Physical review letters* 49, no. 2 (1982): 91.

[48] G. Weihs, T. Jennewein, C. Simon, H. Weinfurter, and A. Zeilinger. "Violation of Bell's inequality under strict Einstein locality conditions." *Physical Review Letters* 81, no. 23 (1998): 5039.

[49] A. Einstein, B. Podolsky, and N. Rosen. "Can quantum-mechanical description of physical reality be considered complete?." *Physical review* 47, no. 10 (1935): 777.

[50] Jian-yu Lu and A. Liu. "An X wave transform." *IEEE Transactions on Ultrasonics, Ferroelectrics, and Frequency Control* 47, no. 6 (2000): 1472-1481.

**Jian-yu Lu** (S'86--M'88--SM'99--F'08) received the B.S. degree in physics/electrical engineering in February 1982 from Fudan University, Shanghai, China; the M.S. degree in physics/acoustics in 1985 from Tongji University, Shanghai, China; and the Ph.D. degree in biomedical engineering in 1988 from Southeast University, Nanjing, China. From December 1988 to February 1990, he was a Postdoctoral Research Fellow at Mayo Medical School, Rochester, Minnesota, USA.

Since 1997, Dr. Lu has been a professor in the Department of Bioengineering at The University of Toledo (UT), Toledo, OH, USA, and since 1998, he has been an adjunct professor in the College of Medicine and Life Sciences. Before joining UT as a professor in 1997, he was an associate professor of biophysics at Mayo Medical School and an Associate Consultant at the Department of Physiology and Biophysics, Mayo Clinic/Foundation, Rochester, MN, USA. His research interests are in acoustic imaging and tissue identification, medical ultrasonic transducers, and ultrasonic beam forming and propagation.

Dr. Lu received the Outstanding Paper Award from the IEEE UFFC Society (UFFC-S) for two of his papers published in the IEEE TUFFC in 1992 for the discovery of X wave that, in theory, can propagate to an infinite distance without spreading (diffraction-free) and has both its phase and group velocities greater than the speed of sound or light in vacuum (superluminal). The X wave has applications in medical imaging (in both ultrasound and optics), optical communications, and physics. In addition, he received the Edward C. Kendall Award for his meritorious research from the Mayo Alumni Association in 1992, the NIH FIRST Award in 1991, Distinguished Service Award from UFFC-S in 2016, and the Engineer of the Year Award from the IEEE Toledo Section in 2021.

Dr. Lu served as the President of IEEE UFFC-S from 2014-2015, the Editor-in-Chief of IEEE TUFFC from 2002-2007, the General Chair of 2008 IEEE IUS, the Technical Program Committee (TPC) Chair of 2001 IEEE IUS, a member of the Editorial Board of IEEE Access from 2016-2021, an Elected AdCom member of IEEE UFFC Society from 2009-2011, and many committees of UFFC-S. In addition, he served in IEEE Toledo Section.

Dr. Lu is a Fellow of IEEE (conferred in 2008), a Fellow of the American Institute of Ultrasound in Medicine (AIUM) (conferred in 2005), and a Fellow of the American Institute for Medical and Biological Engineering (AIMBE) (conferred in 2007).